Yang *et al. Microstructures* 2023;3:2023005
DOI: 10.20517/microstructures.2022.24

Microstructures

Research Article

Open Access

Check for updates

An ultraviolet-visible distinguishable broadband photodetector based on the positive and negative photoconductance effects of a graphene/ZnO quantum dot heterostructure

Xun Yang[#], Chao-Jun Wang[#], Shaobo Cheng, Xi-Gui Yang, Jin-Hao Zang, Chong-Xin Shan

Henan Key Laboratory of Diamond Optoelectronic Materials and Devices, Key Laboratory of Material Physics, Ministry of Education, School of Physics and Microelectronics, Zhengzhou University, Zhengzhou 450052, Henan, China.
[#]Authors contributed equally.

Correspondence to: Dr. Shaobo Cheng, Henan Key Laboratory of Diamond Optoelectronic Materials and Devices, Key Laboratory of Material Physics, Ministry of Education, School of Physics and Microelectronics, Zhengzhou University, Zhengzhou 450052, Henan, China. E-mail: chengshaobo@zzu.edu.cn; Dr. Chong-Xin Shan, Henan Key Laboratory of Diamond Optoelectronic Materials and Devices, Key Laboratory of Material Physics, Ministry of Education, School of Physics and Microelectronics, Zhengzhou University, Zhengzhou 450052, Henan, China. E-mail: cxshan@zzu.edu.cn

How to cite this article: Yang X, Wang CJ, Cheng S, Yang XG, Zang JH, Shan CX. An ultraviolet-visible distinguishable broadband photodetector based on the positive and negative photoconductance effects of a graphene/ZnO quantum dot heterostructure. *Microstructures* 2023;3:2023005. https://dx.doi.org/10.20517/microstructures.2022.24

Received: 6 Sep 2022 **First Decision:** 9 Oct 2022 **Revised:** 21 Oct 2022 **Accepted:** 25 Nov 2022 **Published:** 10 Jan 2023

Academic Editor: Zibin Chen **Copy Editor:** Fangling Lan **Production Editor:** Fangling Lan

Abstract

Broadband photodetectors covering the ultraviolet (UV) to visible range are significant for applications in communication and imaging. Broadband photodetectors with the capacity to distinguish wavelength bands are highly desirable because they can provide additional spectral information. Herein, we report a UV-visible distinguishable broadband photodetector based on a graphene/ZnO quantum dot heterostructure. The photodetector exhibits negative photoconductance under visible illumination because the adsorbents on graphene act as scattering centers to reduce the carrier mobility. In contrast, under UV illumination, the photodetector shows positive photoconductance as the photogenerated electrons in the ZnO quantum dots transfer to the graphene, thereby increasing the conductivity. Thus, the detection and distinction of UV and visible illumination can be realized by utilizing the opposing photoconductivity changes. These results offer inspiration for the design of multifunctional broadband photodetectors.

Keywords: Graphene, ZnO, positive photoconductance, negative photoconductance, broadband photodetector

INTRODUCTION

Photodetectors, which convert optical to electrical signals, play a key role in optoelectronic systems[1-6]. In contrast to photodetectors that respond only to a specific wavelength range, broadband photodetectors can detect light over a broad spectral range and it is therefore essential to various techniques, including image sensing, optical communications, environmental monitoring, and so on[7-9]. Broadband photodetectors responding to light over a wide spectral range from ultraviolet (UV) to infrared have been developed from a variety of materials, such as two-dimensional (2D) materials, perovskites, organic semiconductors, and so on. However, the specific band of the incident light usually cannot be distinguished[10-13]. Therefore, broadband photodetectors with the capacity to distinguish different wavelength bands are highly desirable and can provide additional spectral information. For instance, UV-visible distinguishable broadband photodetectors are required for astronomical detection, information storage and other applications[1,14-16]. However, it is challenging to detect and distinguish UV and visible light using a single photodetector.

Graphene is a promising material for broadband photodetectors due to its wide-range absorption spectrum and high carrier mobility[17-22]. More interestingly, both positive and negative photoconductance responses have been reported for graphene photodetectors[23-25]. Ordinarily, light with photon energy larger than the band gap generates carriers in the valence and conduction bands of a semiconductor material, thereby increasing the conductivity. Such positive photoconductance (PPC) has been observed in most photodetectors[26,27]. In contrast to PPC, the conductivity in some low-dimensional materials may decrease under illumination, i.e., negative photoconductance (NPC)[24,28-30]. This abnormal phenomenon has been observed in photodetectors based on graphene, InAs nanowires, ZnS nanoparticles, carbon nanotubes, monolayer MoS_2, and so on[23,30-32]. NPC in graphene is related to surface adsorbents, which act as scattering centers and decrease the carrier mobility under light illumination, leading to a decrease in conductivity[33,34]. In contrast, graphene photodetectors with PPC and high responsivity can also be obtained from van der Waals heterostructures composed of graphene and other materials[7,35]. The opposing photoconductivity changes of photodetectors with PPC and NPC can be easily distinguished[36]. Therefore, UV-visible distinguishable broadband photodetectors may be realized by integrating the two different response mechanisms in the same photodetector.

Here, we present a UV-visible distinguishable photodetector composed of graphene and zinc oxide (ZnO) quantum dots (QDs). Bare graphene shows NPC under illumination from the UV to visible region. To make the response in the UV and visible region distinguishable, ZnO QDs are coated onto graphene to convert the NPC response under UV illumination to a PPC response. ZnO is chosen to absorb UV illumination due to its wide bandgap (3.3 eV, ~376 nm), low cost and abundant nanostructures[37-42]. Moreover, given that the surface states of ZnO are sensitive to the environment, the applications of ZnO photodetectors may further be extended to the chemical, medical and biological fields[43-48]. In the graphene/ZnO QD van der Waals heterostructure, electrons generated in the ZnO QDs by UV light can transfer to the graphene and enhance its conductivity, resulting in PPC in the UV region. Furthermore, the graphene/ZnO QD photodetector retains the NPC response in the visible region because the ZnO QDs do not absorb visible light. In this context, the graphene/ZnO QD photodetector shows PPC under UV light and NPC under visible light, thereby realizing the detection and distinction of UV and visible illumination simultaneously.

RESULTS AND DISCUSSION

Before investigating the spectral response characteristics of the graphene/ZnO QD photodetector, we first study the photoresponsive behavior of the bare graphene device. A schematic diagram of the bare graphene photodetector is displayed in Figure 1A. In this structure, graphene functions as the charge transport channel as well as the light-absorbing medium. The Raman spectrum of graphene is shown in Figure 1B. The two predominant peaks located at 1583 and 2680 cm^{-1} can be attributed to the graphene G- and 2D-bands, respectively. The small peak at 1344 cm^{-1} is the D-band Raman peak of graphene, related to defects or disorders in the hybrid structure[49,50]. The intensity ratio between the 2D and G peaks is ~0.6, indicating that the graphene is bilayer[51]. Figure 1C demonstrates the photoresponsive behavior of the bare graphene device under UV and visible illumination at a source-drain voltage (V_{DS}) of 0.2 V and a gate voltage (V_G) of 0 V. Under illumination at all wavelengths, the source-drain current (I_{DS}) gradually decreases within 1000 s, indicating persistent NPC. The persistent NPC in graphene derives from the adsorbents (O_2 or OH^- groups) at its surface, which induce p-type conductance and act as scattering centers under illumination, thereby reducing its conductance[24,52]. The decrease in free carrier mobility of graphene under illumination can also be confirmed by Hall measurements. In dark conditions, the hole mobility of graphene is 1050 $cm^2\ V^{-1}\ s^{-1}$, which decreases to 910 $cm^2\ V^{-1}\ s^{-1}$ under 365 nm UV illumination. After the light is switched off, the I_{DS} recovers slowly. For instance, after 4000 s, the current under 365 nm illumination only recovers to 24%[53]. It is notable that both the saturated current and transition time vary with the incident light wavelength, which is related to the wavelength-dependent absorption characteristics of graphene[24,54]. Figure 1D shows the responsivity of the graphene photodetector *vs.* the excitation wavelength. The responsivity is defined as $R = (I_{ph}\text{-}I_{dark})/(P_{ph}*S)$, where I_{ph} is I_{DS} under illumination, I_{dark} is I_{DS} in the dark environment, P_{ph} is the incident light intensity density and S is the active area of the device. The negative responsivity values represent the NPC behavior of the photodetector. The absolute value of the responsivity increases as the excitation wavelength decreases.

To make the response of the photodetector to UV illumination distinguishable from that to visible illumination, the graphene is coated with ZnO QDs to form a graphene/ZnO QD photodetector, as shown in Figure 2A. Figure 2B presents the transmission electron microscopy (TEM) image of the ZnO QDs, which show a typical diameter of ~5 nm. The HRTEM image clearly identifies lattice fringes with a spacing of 0.26 nm, corresponding to the (002) plane of hexagonal wurtzite ZnO[55]. Figure 2C shows the XRD pattern of the ZnO QDs. There are six characteristic peaks, corresponding to the (100), (101), (102), (110), (103) and (200) planes of the hexagonal wurtzite structure of the ZnO QDs (P63mc, $a = b = 0.325$ nm, $c = 0.521$ nm, JCPDS Card No. 80-007). Figure 2D-F show the XPS survey, O 1s and Zn 2p spectra of the ZnO QDs. The O 1s spectrum is composed of three peaks at 530.8, 532.0 and 534.0 eV, corresponding to Zn-O, O-C=O and C-O-C/OH bonds, respectively[56]. The XPS spectrum for Zn 2p shows two peaks at 1023.4 and 1046.5 eV, which can be attributed to Zn $2p_{3/2}$ and Zn $2p_{1/2}$, respectively, thereby confirming the divalent state of Zn. Figure 2G shows the Raman spectrum of the graphene/ZnO QDs. In addition to the peaks from graphene, there are three obvious peaks at 99, 418 and 640 cm^{-1}, which derive from the E2(low), E1(TO) and multi-phonon modes of ZnO, respectively[57,58]. Figure 2H presents the absorption of the graphene/ZnO QDs, which show an absorption edge at ~376 nm, corresponding to the bandgap of ZnO. The absorption in the visible region is due to scattering by the ZnO QDs.

Figure 3A shows the response characteristics of the graphene/ZnO QD photodetector under UV (upper panel) and visible (lower panel) illumination. NPC behavior can be observed under visible illumination, similar to that of the bare graphene photodetector. However, under UV illumination, the I_{DS} increases gradually, indicating PPC response to UV illumination. After the light is switched off, the I_{DS} recovers to its original level slowly. The current under 650 nm illumination recovers to 21% after 1400 s, while the current

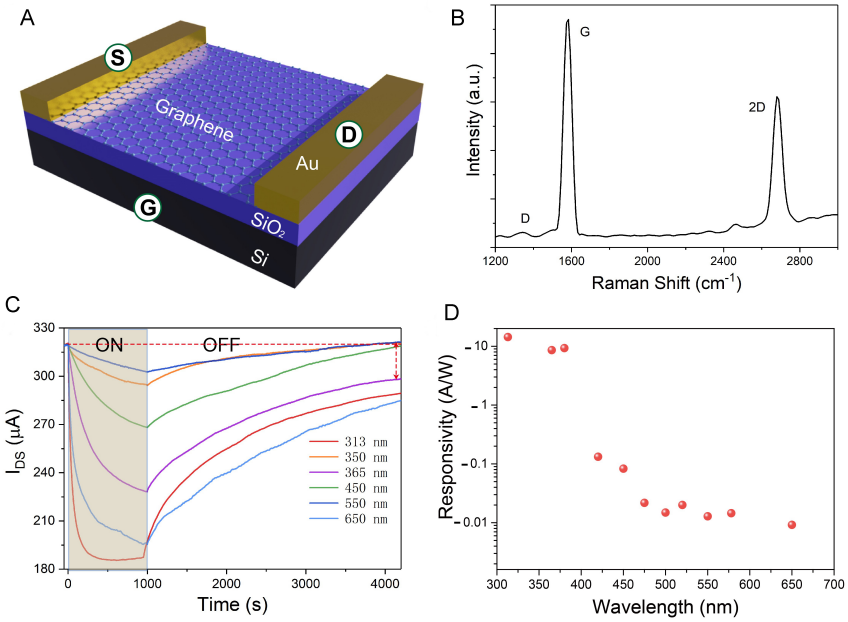

Figure 1. Bare graphene photodetector. (A) Schematic diagram of device structure (device area is 100 μm in length and 1200 μm in width defined as the area between the two electrodes). (B) Raman spectrum of graphene. (C) Photoelectric on/off response under illumination in the UV to visible range (*VDS* = 0.2 V and *VG* = 0 V). (D) Responsivity at different wavelengths.

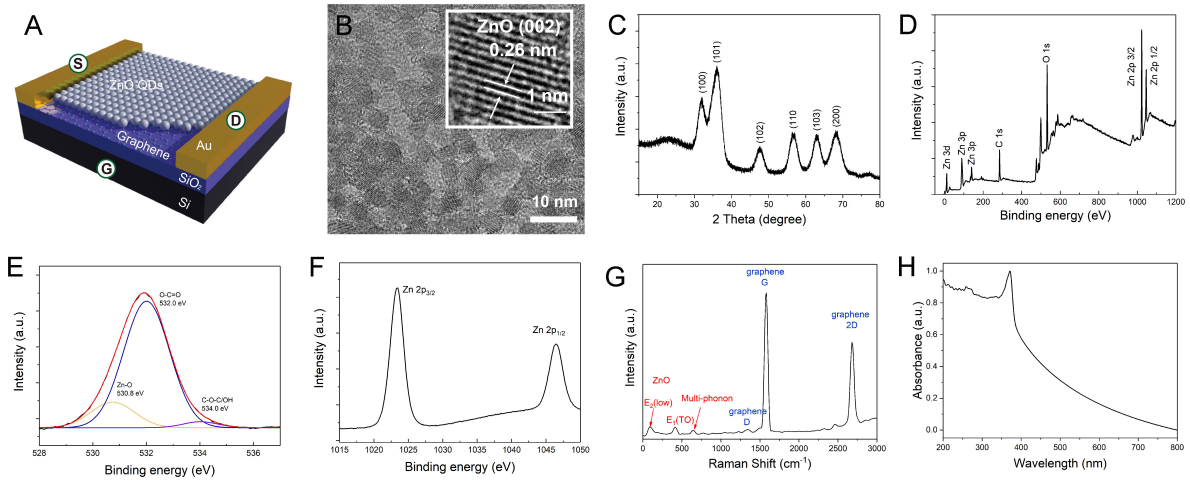

Figure 2. Graphene/ZnO QD heterostructure. (A) Schematic diagram of graphene/ZnO QD heterostructure. (B) TEM image of ZnO QDs. Inset shows HRTEM image of a single ZnO QD. (C) XRD pattern of ZnO QDs. (D) XPS survey spectrum and high-resolution spectra of (E) O 1s and (F) Zn 2p for ZnO QDs. (G) Raman and (H) absorption spectra of graphene/ZnO QDs.

under 313 nm illumination recovers to 4% after 700 s. The opposing photoconductance changes under UV and visible illumination confirm the spectrum-selective detection of the graphene/ZnO QD device. Figure 3B and C show the time-dependent response curves of the graphene/ZnO QD photodetector under 365 and 460 nm illumination, respectively. The light sources are turned on and off periodically to investigate the reproducibility of the photoresponse. Both the PPC and NPC responses are repeatable. However, the baselines change slightly after multicycle testing, which may derive from catalytic modification of the graphene.

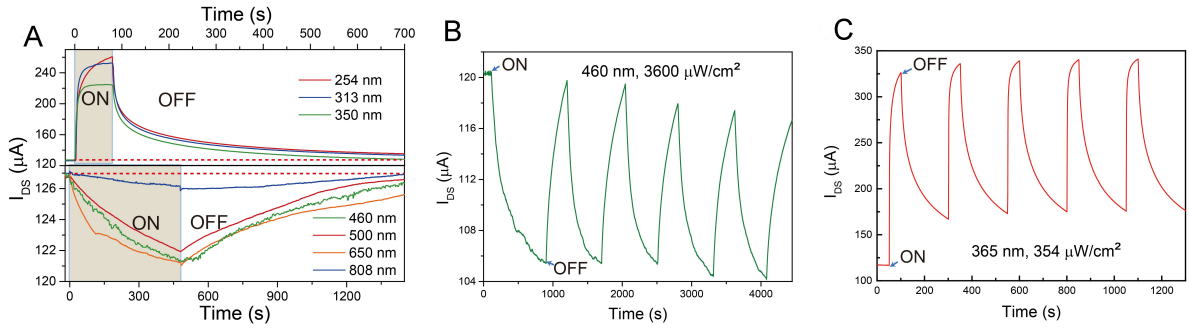

Figure 3. Graphene/ZnO QD photodetector. (A) Photocurrent response under UV and visible illumination (*VDS* = 0.2 V and *VG* = 0 V). Time-dependent photoresponse of photodetector under (B) 460 and (C) 365 nm illumination (*VDS* = 0.2 V and *VG* = 0 V).

Figure 4A and B plot the responsivity of the graphene/ZnO QD photodetector as a function of light intensity. The responsivity decreases with the light intensity and the data can be fitted using $R \propto E^{\beta-1}$, where E is the light intensity and β is a constant[25]. The constant β values under visible (460 nm) and UV (365 nm) illumination are fitted to be 0.46 and 0.12, respectively. The different β values suggest different trap states for NPC under visible illumination and PPC under UV illumination[59].

To obtain a better understanding of the response mechanism of the graphene/ZnO QD photodetector, we measured the transfer curves under UV (365 nm) and visible (460 nm) illumination, as shown in Figure 5A and B, respectively. In dark conditions, the transfer curve shows typical ambipolar transfer characteristics with the Dirac point at 1.7 V, due to the p-type doping effects from surface adsorbents. Under 460 nm illumination, the transfer curve shifts down, confirming the NPC response of the photodetector. Moreover, the Dirac point shifts gradually to 2.0 V with the incident light intensity increasing to 128 μW/cm^2, indicating that the photogenerated electrons are trapped, which is also regarded as the photogating effect[59]. In contrast, the Dirac point moves to about -0.9 V under 365 nm illumination. The negative Dirac point indicates that the p-type conductivity of graphene turns into n-type conductivity because the photogenerated electrons in the ZnO QDs transfer to the graphene[42,60]. The electron transfer mechanism can be understood using the schematic diagram in Figure 5C. Under illumination with photon energy larger than the bandgap of ZnO, electrons and holes are generated in the ZnO QDs. The photogenerated holes are trapped by surface hole traps formed by adsorbed oxygen ions, which are sufficient due to the high surface-to-volume ratio of the ZnO QDs[15,42,61,62]. Furthermore, the photogenerated electrons transfer to the graphene, which are numerous enough to compensate for the holes in the graphene and convert the p- to n-type conductivity. Hall measurements also show that the hole sheet density and mobility of graphene coated with ZnO QDs in the dark are 6.39×10^{12} cm^{-2} and 360 cm^2 V^{-1} s^{-1}, respectively. The carrier mobility is smaller than that of the bare graphene (1050 cm^2 V^{-1} s^{-1}) due to scattering by the ZnO QDs. Under the illumination of 365 nm light with an intensity of 20 μW/cm^2, the graphene exhibits n-type conductivity with an electron sheet density of 1.6×10^{13} cm^{-2} and a mobility of 150 cm^2 V^{-1} s^{-1}. The significant increase in carrier density under UV illumination results in an increase in conductivity, namely, PPC.

Figure 5D shows the responsivity spectrum of the graphene/ZnO QD photodetector accompanied by the absorption spectrum of the ZnO QDs. The absorption edge of the ZnO QDs (376 nm) is denoted by the vertical dashed line. It is apparent that the graphene/ZnO QD photodetector shows PPC under illumination with photon energy larger than the bandgap of the ZnO QDs, because a large amount of photon-generated electrons transfer from the ZnO QDs to the graphene, thereby increasing the conductivity. Furthermore, under illumination with photon energy smaller than the bandgap of the ZnO QDs, photoinduced impurity

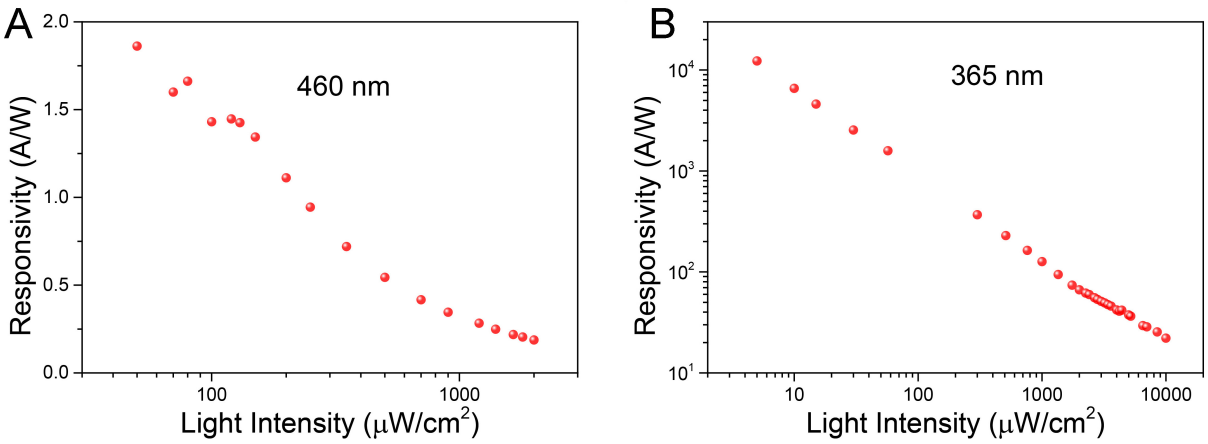

Figure 4. Responsivity of graphene/ZnO QD photodetector as a function of light intensity for (A) 460 and (B) 365 nm illumination.

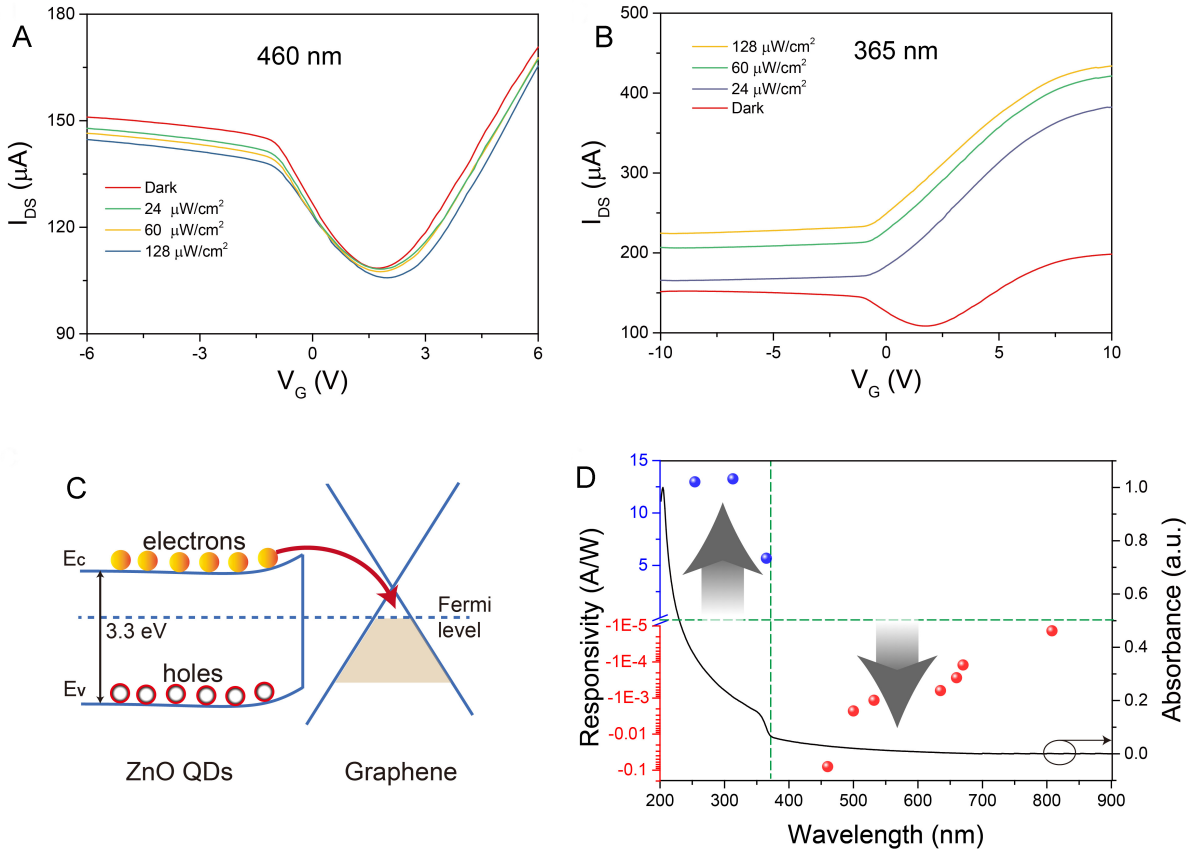

Figure 5. Photoresponsive behavior of graphene/ZnO QD photodetector. Transfer curves under (A) 460 and (B) 365 nm illumination (*VDS* = 0.2 V). (C) Schematic diagram of charge transfer process between ZnO QDs and graphene. (D) Responsivity spectrum of graphene/ZnO QD photodetector and absorption spectrum of ZnO QDs.

scattering plays the leading role, resulting in NPC. Thus, in this context, the NPC response of the graphene for UV illumination can be converted to a PPC response, thereby realizing the detection and distinction of UV and visible light using a single graphene/ZnO QD photodetector.

CONCLUSIONS

In conclusion, we have demonstrated a UV-visible distinguishable broadband photodetector utilizing the NPC and PPC response in a graphene/ZnO QD heterostructure. The photoresponsive mechanism of the photodetector under visible illumination is attributed to adsorbents on the graphene, which act as scattering centers in illumination conditions to decrease the conductivity. In contrast, under UV illumination, the photogenerated electrons in the ZnO QDs could transfer to the graphene, leading to an increase in conductivity. Thus, the current of the graphene/ZnO QDs photodetector decreases under visible illumination and increases under UV illumination, which can be used to detect and distinguish UV and visible illumination. Our results may expand the application area of broadband photodetectors.

MATERIALS AND METHODS

Device Fabrication: Graphene was grown on copper foils via a chemical vapor deposition method and transferred to Si(n+)/SiO_2 (300 nm) substrates via the solution method. Then, two Ti/Au electrodes were prepared onto the graphene by thermal evaporation using a mask. Another Ti/Au electrode was deposited on the Si substrate as a gate electrode [Figure 1A]. The device active area is 100 μm in length and 1200 μm in width defined as the area between the two electrodes. ZnO QDs were synthesized by a traditional sol-gel method using zinc acetate and KOH as reactants. To fabricate the graphene/ZnO QD photodetector, the ZnO QDs dispersed in an ethanol solution (2 mg/mL) were spin-coated over the graphene at 2000 rpm for 20 s and baked at 70 °C for 10 min. This process was repeated three times to ensure that the graphene was covered by sufficient ZnO QDs. The final thickness of the ZnO QD film is ~120 nm.

Device Characterization: The electrical transport characteristics of the device were studied using a semiconductor characterization system (Keithley 4200-SCS). Handhold lasers and LEDs with different wavelengths were employed as the light sources. The X-ray diffraction (XRD) pattern of the ZnO QDs was obtained using a diffractometer (X'Pert Pro, PANalytical). The Raman spectra were recorded using an SOL instrument spectrometer (Confotec MR520) using a 532-nm laser as the excitation source. X-ray photoelectron spectroscopy (XPS) spectra were carried out using an XPS spectrometer (Thermo ESCALAB 250) and calibrated based on the C 1s peak at 284.8 eV. The absorption spectra of the ZnO QDs were measured using a spectrophotometer (Hitachi UH4150). The morphology of the ZnO QDs was investigated using transmission electron microscopy (TEM, JEOL 2100). All the photoresponsive measurements were carried out at room temperature and in air.

DECLARATIONS

Authors' contributions

Design, writing review and editing: Yang X, Cheng S, Shan CX
Data analysis: Yang X, Yang XG, Cheng S
Data acquisition: Yang X, Wang CJ
Sample fabrication: Wang CJ, Zang JH

Availability of data and materials

Not applicable.

Financial support and sponsorship

This work was supported by National Natural Science Foundation of China (Nos. 62271450, 12174348) and Henan Center for Outstanding Overseas Scientists (No. GZS201903).

Conflicts of interest

All authors declared that there are no conflicts of interest.

Ethical approval and consent to participate

Not applicable.

Consent for publication

Not applicable.

REFERENCES

1. Du S, Lu W, Ali A, et al. A broadband fluorographene photodetector. *Adv Mater* 2017;29:1700463. DOI PubMed
2. Clifford JP, Konstantatos G, Johnston KW, Hoogland S, Levina L, Sargent EH. Fast, sensitive and spectrally tuneable colloidal-quantum-dot photodetectors. *Nat Nanotechnol* 2009;4:40-4. DOI PubMed
3. Patel M, Kumar M, Kim J. Polarity flipping in an isotype heterojunction (p-SnS/p-Si) to enable a broadband wavelength selective energy-efficient photodetector. *J Mater Chem C* 2018;6:6899-904. DOI
4. Bao C, Yang J, Bai S, et al. High performance and stable all-inorganic metal halide perovskite-based photodetectors for optical communication applications. *Adv Mater* 2018;30:e1803422. DOI PubMed
5. Li Y, Shi Z, Li X, Shan C. Photodetectors based on inorganic halide perovskites: materials and devices. *Chinese Phys B* 2019;28:017803. DOI
6. Guo Q, Pospischil A, Bhuiyan M, et al. Black phosphorus mid-infrared photodetectors with high gain. *Nano Lett* 2016;16:4648-55. DOI PubMed
7. Liu CH, Chang YC, Norris TB, Zhong Z. Graphene photodetectors with ultra-broadband and high responsivity at room temperature. *Nat Nanotechnol* 2014;9:273-8. DOI PubMed
8. Rogalski A. Infrared detectors: status and trends. *Prog Quantum Electron* 2003;27:59-210. DOI
9. Clark J, Lanzani G. Organic photonics for communications. *Nat Photon* 2010;4:438-46. DOI
10. Ding N, Wu Y, Xu W, et al. A novel approach for designing efficient broadband photodetectors expanding from deep ultraviolet to near infrared. *Light Sci Appl* 2022;11:91. DOI PubMed PMC
11. Li C, Wang H, Wang F, et al. Ultrafast and broadband photodetectors based on a perovskite/organic bulk heterojunction for large-dynamic-range imaging. *Light Sci Appl* 2020;9:31. DOI PubMed PMC
12. Yao J, Yang G. 2D material broadband photodetectors. *Nanoscale* 2020;12:454-76. DOI PubMed
13. Nanda Kumar Reddy N, Godavarthi S, Mohan Kumar K, et al. Evaluation of temperature dependent electrical transport parameters in Fe_3O_4/SiO_2/n-Si metal-insulator-semiconductor (MIS) type Schottky barrier heterojunction in a wide temperature range. *J Mater Sci Mater Electron* 2019;30:8955-66. DOI
14. Chesnokov S, Dolzhenko D, Ivanchik I, Khokhlov D. Far infrared high-performance lead telluride-based photodetectors for space-born applications. *Infrared Phys Technol* 1994;35:23-31. DOI
15. Kind H, Yan HQ, Messer B, Law M, Yang PD. Nanowire ultraviolet photodetectors and optical switches. *Adv Mater* 2002;14:158-60. DOI
16. Schaffer M, Mitkas P. Requirements and constraints for the design of smart photodetector arrays for page-oriented optical memories. *IEEE J Select Topics Quantum Electron* 1998;4:856-65. DOI
17. Hu W, Li Q, Chen X, Lu W. Recent progress on advanced infrared photodetectors. *Acta Phys Sin* 2019;68:35. DOI
18. Long M, Wang P, Fang H, Hu W. Progress, challenges, and opportunities for 2D material based photodetectors. *Adv Funct Mater* 2019;29:1803807. DOI
19. Zhang X, John S. Broadband light-trapping enhancement of graphene absorptivity. *Phys Rev B* 2019:99. DOI
20. Jia W, Ren P, Tian Y, Fan C. Dynamically tunable optical properties in graphene-based plasmon-induced transparency metamaterials. *Chinese Phys B* 2019;28:026102. DOI
21. Xia C, Xue B, Wang T, Peng Y, Jia Y. Interlayer coupling effects on Schottky barrier in the arsenene-graphene van der Waals heterostructures. *Appl Phys Lett* 2015;107:193107. DOI
22. Du H, Jia Y, Sun Q, Guo Z. Single vacancy defects diffusion at the initial stage of graphene growth: a first-principles study. *Phys Lett A* 2015;379:1270-3. DOI
23. Cui B, Xing Y, Han J, et al. Negative photoconductivity in low-dimensional materials. *Chinese Phys B* 2021;30:028507. DOI
24. Biswas C, Güneş F, Duong DL, et al. Negative and positive persistent photoconductance in graphene. *Nano Lett* 2011;11:4682-7. DOI PubMed
25. Sun Z, Liu Z, Li J, Tai GA, Lau SP, Yan F. Infrared photodetectors based on CVD-grown graphene and PbS quantum dots with

ultrahigh responsivity. *Adv Mater* 2012;24:5878-83. DOI PubMed
26. Nakanishi H, Bishop KJ, Kowalczyk B, et al. Photoconductance and inverse photoconductance in films of functionalized metal nanoparticles. *Nature* 2009;460:371-5. DOI PubMed
27. Hayden O, Agarwal R, Lieber CM. Nanoscale avalanche photodiodes for highly sensitive and spatially resolved photon detection. *Nat Mater* 2006;5:352-6. DOI PubMed
28. Han Y, Zheng X, Fu M, et al. Negative photoconductivity of InAs nanowires. *Phys Chem Chem Phys* 2016;18:818-26. DOI PubMed
29. Wei P, Chattopadhyay S, Yang M, et al. Room-temperature negative photoconductivity in degenerate InN thin films with a supergap excitation. *Phys Rev B* 2010:81. DOI
30. Chen X, Xu Y, Zhou D, et al. Solar-blind photodetector with high avalanche gains and bias-tunable detecting functionality based on metastable phase α-Ga_2O_3/ZnO Isotype Heterostructures. *ACS Appl Mater Interfaces* 2017;9:36997-7005. DOI
31. Wu JY, Chun YT, Li S, et al. Broadband MoS_2 field-effect phototransistors: ultrasensitive visible-light photoresponse and negative infrared photoresponse. *Adv Mater* 2018;30:1705880. DOI PubMed
32. Yang Y, Peng X, Kim HS, et al. Hot carrier trapping induced negative photoconductance in inas nanowires toward novel nonvolatile memory. *Nano Lett* 2015;15:5875-82. DOI PubMed
33. Tielrooij KJ, Song JCW, Jensen SA, et al. Photoexcitation cascade and multiple hot-carrier generation in graphene. *Nat Phys* 2013;9:248-52. DOI
34. Nomura K, MacDonald AH. Quantum hall ferromagnetism in graphene. *Phys Rev Lett* 2006;96:256602. DOI PubMed
35. Kong WY, Wu GA, Wang KY, et al. Graphene-β-Ga_2O_3 heterojunction for highly sensitive deep UV Photodetector application. *Adv Mater* 2016;28:10725-31. DOI PubMed
36. Haque MA, Li J, Abdelhady AL, et al. Transition from positive to negative photoconductance in doped hybrid perovskite semiconductors. *Adv Opt Mater* 2019;7:1900865. DOI
37. Yang X, Ni P, Jing P, et al. Room temperature electrically driven ultraviolet plasmonic lasers. *Adv Opt Mater* 2019;7:1801681. DOI
38. Yang X, Shan CX, Ni PN, et al. Electrically driven lasers from van der Waals heterostructures. *Nanoscale* 2018;10:9602-7. DOI PubMed
39. Lu Y, Shi Z, Shan C, Shen D. ZnO-based deep-ultraviolet light-emitting devices. *Chinese Phys B* 2017;26:047703. DOI
40. Shi ZF, Xu TT, Wu D, et al. Semi-transparent all-oxide ultraviolet light-emitting diodes based on ZnO/NiO-core/shell nanowires. *Nanoscale* 2016;8:9997-10003. DOI PubMed
41. Shi ZF, Sun XG, Wu D, et al. High-performance planar green light-emitting diodes based on a PEDOT:PSS/$CH_3NH_3PbBr_3$/ZnO sandwich structure. *Nanoscale* 2016;8:10035-42. DOI PubMed
42. Guo W, Xu S, Wu Z, Wang N, Loy MM, Du S. Oxygen-assisted charge transfer between ZnO quantum dots and graphene. *Small* 2013;9:3031-6. DOI PubMed
43. Liu X, Yang Y, Xing X, Wang Y. Grey level replaces fluorescent intensity: fluorescent paper sensor based on ZnO nanoparticles for quantitative detection of Cu_{2+} without photoluminescence spectrometer. *Sensor Actuat B Chem* 2018;255:2356-66. DOI
44. Barui AK, Veeriah V, Mukherjee S, et al. Zinc oxide nanoflowers make new blood vessels. *Nanoscale* 2012;4:7861-9. DOI PubMed
45. Kim K, Kim H, Choi K, Kim H, Lee J. ZnO hierarchical nanostructures grown at room temperature and their C_2H_5OH sensor applications. *Sensor Actuat B Chem* 2011;155:745-51. DOI
46. Pichat P. Powder photocatalysts: characterization by isotopic exchanges and photoconductivity; potentialities for metal recovery, catalyst preparation and water pollutant removal. In Schiavello M. editor, Photocatalysis and environment: trends and applications. Dordrecht: Springer Netherlands. 1988. pp 399-424.
47. Tan Y, Qiao Q, Weng T, et al. Self-powered photodetector based on poly(3-hexylthiophene)/Zinc oxide quantum dots Organic-inorganic hybrid heterojunction. *Chem Phys Lett* 2022;806:140033. DOI
48. Zhou YH, Zhang ZB, Xu P, Zhang H, Wang B. UV-visible photodetector based on I-type heterostructure of ZnO-QDs/monolayer MoS_2. *Nanoscale Res Lett* 2019;14:364. DOI PubMed PMC
49. Zhang J, Zhang X, Ding Y, Zhu Y. ZnO/graphene/Ag composite as recyclable surface-enhanced Raman scattering substrates. *Appl Opt* 2016;55:9105-12. DOI PubMed
50. Zhang BY, Liu T, Meng B, et al. Broadband high photoresponse from pure monolayer graphene photodetector. *Nat Commun* 2013;4:1811. DOI PubMed
51. Zhou H, Qiu C, Yu F, et al. Thickness-dependent morphologies and surface-enhanced raman scattering of Ag deposited on n-layer graphenes. *J Phys Chem C* 2011;115:11348-54. DOI
52. Wang Q, Tu Y, Ichii T, et al. Decoration of reduced graphene oxide by gold nanoparticles: an enhanced negative photoconductivity. *Nanoscale* 2017;9:14703-9. DOI PubMed
53. Bhatt V, Kumar M, Kim J, Chung H, Yun J. Persistent photoconductivity in Al-doped ZnO photoconductors under air, nitrogen and oxygen ambiance: role of oxygen vacancies induced DX centers. *Ceram Int* 2019;45:8561-70. DOI
54. Wang Y, Ni Z, Liu L, et al. Stacking-dependent optical conductivity of bilayer graphene. *ACS Nano* 2010;4:4074-80. DOI PubMed
55. Fernando JFS, Zhang C, Firestein K, Nerkar JY, Golberg DV. ZnO quantum dots anchored in multilayered and flexible amorphous carbon sheets for high performance and stable lithium ion batteries. *J Mater Chem A* 2019;7:8460-71. DOI
56. Zhou Z, Pourhashem S, Wang Z, Duan J, Zhang R, Hou B. Distinctive roles of graphene oxide, ZnO quantum dots, and their nanohybrids in anti-corrosion and anti-fouling performance of waterborne epoxy coatings. *Chem Eng J* 2022;439:135765. DOI
57. Nowak E, Szybowicz M, Stachowiak A, et al. A comprehensive study of structural and optical properties of ZnO bulk crystals and

polycrystalline films grown by sol-gel method. *Appl Phys A* 2020:126. DOI

58. Kim HH, Lee Y, Lee YJ, et al. Realization of excitation wavelength independent blue emission of ZnO quantum dots with intrinsic defects. *ACS Photonics* 2020;7:723-34. DOI
59. Han J, Wang J, Yang M, et al. Graphene/Organic semiconductor heterojunction phototransistors with broadband and bi-directional photoresponse. *Adv Mater* 2018;30:e1804020. DOI PubMed
60. Williams G, Kamat PV. Graphene-semiconductor nanocomposites: excited-state interactions between ZnO nanoparticles and graphene oxide. *Langmuir* 2009;25:13869-73. DOI PubMed
61. Li QH, Gao T, Wang YG, Wang TH. Adsorption and desorption of oxygen probed from ZnO nanowire films by photocurrent measurements. *Appl Phys Lett* 2005;86:123117. DOI
62. Fan Z, Chang P, Lu JG, et al. Photoluminescence and polarized photodetection of single ZnO nanowires. *Appl Phys Lett* 2004;85:6128-30. DOI